Evolution of the millimeter-wave collective Thomson scattering system of the high-field tokamak Frascati Tokamak Upgrade

U. Tartari,[a] G. Grosso, G. Granucci, F. Gandini, S. Garavaglia, G. Grossetti, A. Simonetto, V. Mellera, and V. Muzzini
Istituto di Fisica del Plasma, CNR-ENEA-Euratom Association, Via R. Cozzi 53, 20125 Milano, Italy

L. Lubyako and A. Shalashov
Institute of Applied Physics, Russian Academy of Sciences, Ulyanova Street 46, 603950 Nizhny Novgorod, Russian Federation

F. P. Orsitto and G. Ciccone
CRE-ENEA, Euratom-ENEA Association, Via E. Fermi 45, 00044 Frascati, Italy

F. Volpe[b]
Culham Science Centre, UKAEA-EURATOM Association, Abingdon, Oxfordshire, OX14 3DB, United Kingdom

(Received 6 December 2006; accepted 26 February 2007; published online 16 April 2007)

We first describe the improved receiving system of the diagnostic experiment of millimeter-wave collective Thomson scattering being run on the Frascati Tokamak Upgrade (FTU), and then discuss some peculiar problems and new operating procedures related to the investigation of strong anomalous spectra of nonthermal origin, many-orders-of-magnitude stronger than the ion thermal feature merged in them, systematically observed in the experimentation, and finally ascribed to a perturbation of the gyrotron that generates the probing beam. Arguments in favor of a more general valence of the solutions actuated for the specific case of FTU are finally given. © *2007 American Institute of Physics.* [DOI: 10.1063/1.2719197]

I. INTRODUCTION

Considerable experimental efforts were devoted in collective Thomson scattering (CTS) on the Frascati Tokamak Upgrade (FTU) device,[1] a proof-of-principle experiment performed in the propagation window below the electron cyclotron (EC) resonance ($f_{gyr}<f_{ec}$) using a $f_{gyr}=140$ GHz ($\lambda_{gyr}=2.1$ mm) gyrotron with nominal output power of 400 kW, to investigate strong anomalous spectra of nonthermal origin that were detected both in aligned- and misaligned-antenna conditions at spectral power densities orders-of-magnitude higher than those of the ion thermal spectra. A strong impulse to the investigation of these spectra came from the consideration that, FTU being one of the very few high-field tokamaks (toroidal magnetic field: $B_T \leq 8$ T) presently in operation, our experiment was the only one carried out in the propagation window of interest for the demonstration of a diagnostic of the *confined* alphas for the future International Thermonuclear Experimental Reactor (ITER).[2]

As discussed in a dedicated article,[3] the anomalous spectra in question were unambiguously interpreted as stray-radiation spectra associated with perturbed gyrotron conditions caused by the back-reflection in the access port of the power fraction polarized in the extraordinary (X) mode in the gyrotron beam injected in the plasma to produce the scattering. The presence of both the right-handed (RH) cutoff for the X mode and the electron-cyclotron (EC) and upper hybrid (UH) layers in the beam injection port is unavoidable in CTS with $f_{gyr}<f_{ec}$. The risk of gyrotron perturbation therefore is quite general in this configuration. Special provisions such as the use of evacuated transmitting antennas must be taken to prevent it.

We recall that in millimeter-wave CTS on thermal density fluctuations a comparatively very small signal scattered by a high-power beam injected in the plasma by a transmitting antenna is collected along the line of sight assigned by a receiving antenna and then spectrally analyzed using a high-sensitivity multichannel heterodyne receiver. The goal is inferring spatially- and temporally resolved information on the ion velocity distribution. In particular, the ion temperature (T_i) is obtained under a Maxwellian assumption. While measuring T_i was also the initial goal of CTS in FTU, in recent years the mission of the experiment has been refocused on performing high-density CTS in the X mode, as of interest for ITER, looking at the T_i measurements as the simplest way for demonstrating this goal. The layout of the CTS experiment in FTU is schematically shown in Fig. 1.

In this work, after a brief recall of some basic principles of CTS and essential information on the layout (Sec. II), we describe the improved receiving system (Sec. III), the peculiar difficulties encountered (Sec. IV), and the operating procedures (Sec. V) expressly developed to make the system cope with the necessities of the investigation of the anoma-

[a]Electronic mail: tartari@ifp.cnr.it
[b]Present address: General Atomics, P. O. Box 85608, San Diego, CA 92186-5608.

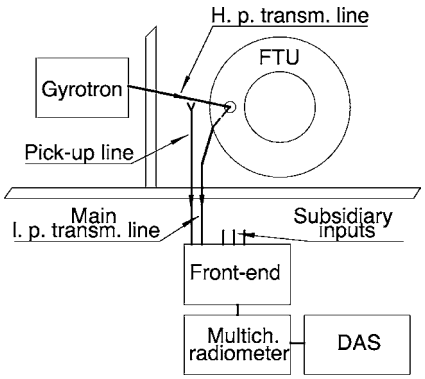

FIG. 1. Schematic of the CTS experiment in FTU. The auxiliary pick-up line and the multi-input front end described in the following are also shown.

lous spectra. Arguments in favor of a more general valence of the solutions proposed are finally given in Sec. VI.

II. CTS BACKGROUND

The wave vector and the frequency of the incident radiation $(\mathbf{k}_i,\lambda_i)$, the scattered radiation $(\mathbf{k}_s,\lambda_s)$, and the plasma-density fluctuation producing the scattered signal $(\mathbf{k},\lambda)$ are related by the conservation rules $\mathbf{k}=\mathbf{k}_s-\mathbf{k}_i$ and $\omega=\omega_s-\omega_i$. At millimeter wavelengths and in the parameters' range of fusion-relevant plasmas, the collective scattering condition $1/k\lambda_D>1$, with $k=|\mathbf{k}|$ and λ_D the Debye length, is satisfied without significant limitations on the scattering angle.

The power scattered per unit frequency and unit solid angle is[4]

$$P_s(\omega) \propto r_e^2 P_{\text{in}} n_i S(\mathbf{k},\omega),$$

with r_e the classical electron radius, n_i the ion density, P_{in} the incident power, and $S(\mathbf{k},\omega)$ the spectral density function. The latter is related to the unidimensional ion velocity distribution in the $\mathbf{k}$ direction by the relation

$$S(\mathbf{k},\omega) \propto |G_e/\varepsilon_{\text{pl}}|^2 f_i(v), \tag{1}$$

with $v=\omega/k$, $\varepsilon_{\text{pl}}=1+G_e+G_i$ the plasma dielectric function, and $G_{e,i}$ the electron and ion susceptibilities, respectively. Relation (1) shows that the CTS spectrum is but a distorted representation of $f_i(v)$. The information on the latter is inferred by best-fitting the data with model spectra. We also see that, being strictly related to $S(\mathbf{k},\omega)$, the information on the ion velocity distribution is mostly contained in the spectral shape and width.

For Maxwellian plasmas, the CTS spectrum is symmetrically distributed about the probing frequency, f_{gyr}, and its half-width can be written as

$$\Delta f_{\text{CTS}} \cong 4c^{-1} m_i^{-1/2} (T_i + Z_{\text{eff}} T_e)^{1/2} f_{\text{gyr}} \sin\,\theta/2, \tag{2}$$

with m_i the ion mass, Z_{eff} the effective ion charge, and θ the scattering angle determined by the geometry. Because of the mass dependence in (2), the contributions from the plasma impurities always present in real plasmas are narrower the heavier their mass, and therefore tend to concentrate in the low-frequency part of the global spectrum one measures, significantly affecting it. This makes detailed analysis of this low-frequency part of outstanding importance in ion thermal CTS.

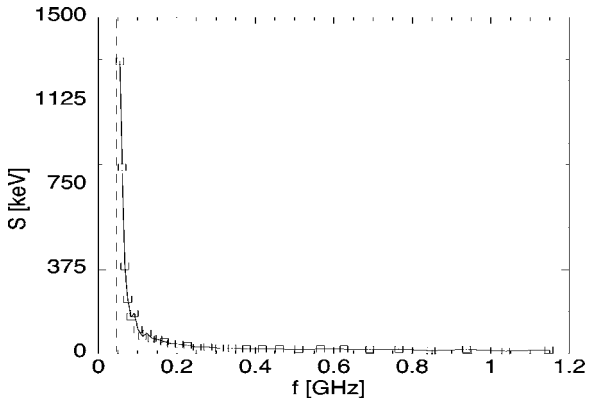

FIG. 2. Example of anomalous spectrum exhibiting a strong feature at low frequency. Shot No. 27148: $B_{T0}=7$ T, $P_{\text{gyr}}=274$ kW, $n_{e,\text{line}}=0.65\times10^{20}$ m^{-3}, $T_{e0}=2.5$ keV.

For deuterium (D) plasmas, the temperature range $(T_i<T_e\cong1-2$ keV) and the scattering angle $(\theta\cong90°)$ available in FTU one typically has $\Delta f_{\text{CTS}}\approx300-500$ MHz. In the temperature scale currently used, which accounts for the CTS signal being statistically narrow-band noise, the maximum of the spectral power density is in the range 100–500 eV. Apart from a shoulder, or in some circumstances a peak, at a frequency approaching the ion-acoustic frequency the spectral shape is monotonically decreasing.

A few examples of anomalous spectra will be sufficient to characterize them and emphasize the big difference between these spectra and the ion thermal spectra briefly described above. The spectrum shown in Fig. 2 only exhibits a strong monotonic low-frequency feature with shape following an inverse power law, $S\propto f^{-\alpha}$, with $\alpha=1-2$. This shape makes it approach the spectrum of the gyrotron noise in normal (nonperturbed) conditions. However, the spectral strength exceeds that typical of the latter by about 5 orders of magnitude. In the spectrum shown in Fig. 3 a more complex, and possibly non-fully resolved, line pattern also appears besides the smooth low-frequency feature of Fig. 2. The scale of the spectral strength now is about 20 times smaller than in

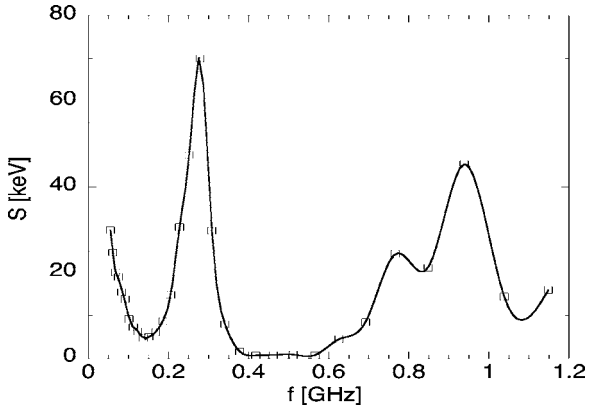

FIG. 3. Anomalous spectrum exhibiting line structures both at low and high frequency besides the smooth, low-frequency feature seen in the spectrum of Fig. 2. The latter is common to all the anomalous spectra. Shot No. 27359: $B_{T0}=7$ T, $P_{\text{gyr}}=307$ kW, $n_{e,\text{line}}=0.75\times10^{20}$ m^{-3}, $T_{e0}=2$ keV.

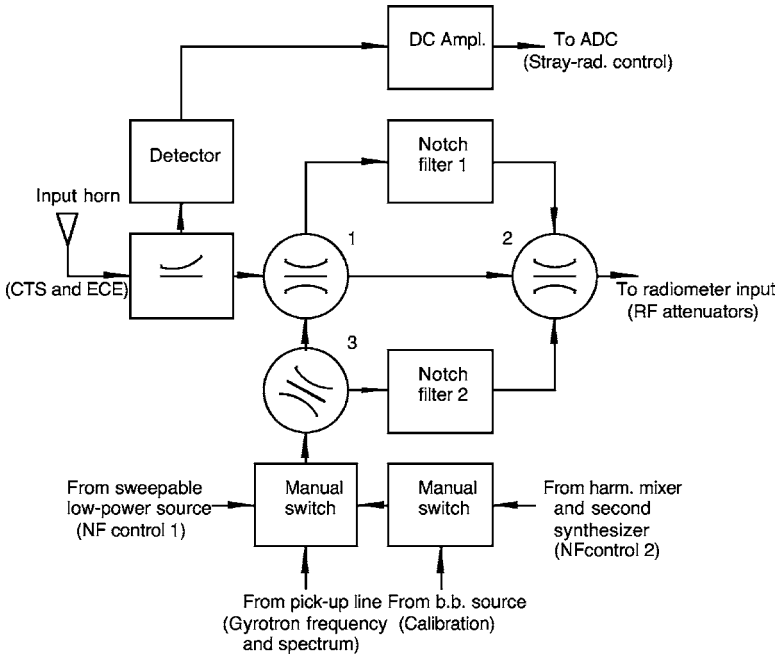

FIG. 4. Block scheme of the multi-input front end of the CTS receiver.

the previous spectrum, but nevertheless still from 2 to 3 orders of magnitude higher than that typical for the ion thermal feature.

Two further points are worth being stressed concerning the anomalous spectra. First, we anticipate that their detection did not imply a variation of the stray-radiation level, as measured by a dedicated monitor set at the receiver input (see the following), with respect to the level detected in shots performed in the vacuum vessel. This contributed to showing that the anomalous spectra were not originated in the plasma. Second, in CTS conditions the plasma target being nearly transparent, the spectra are detected as a result of the multiple reflections undertaken by the unabsorbed gyrotron beam power on the tokamak walls, independently of CTS geometry, and therefore the spectral strengths measured are attenuated by antenna decoupling with respect to their original strength in the interaction region. Antenna decoupling, defined by the ratio P_{gyr}/P_{str}, with P_{gyr} the injected power level and P_{str} the stray-radiation level, in the FTU case is $\geq$50 dB. Together with the line structures exhibited, the huge spectral strengths this implies make the anomalous spectra quite similar to the spectra that would have been observed in the presence of unwanted coherent plasma-wave processes competing with ion thermal CTS.

Since detailed information on the layout and the scattering geometry is not strictly required in the present context, we just recall that in CTS in FTU (a) the propagation is markedly oblique with respect to the magnetic-field direction and therefore the polarization of the two plasma modes elliptic;[5] (b) as it is generally the case, the partition in normal modes of the linearly polarized beam we currently used in the experimentation is different in the beam injection port and in the plasma, the beam propagation angle with respect to the magnetic-field direction being different in the two cases. As already mentioned, the presence of a non-negligible power fraction polarized in the *X* mode in the beam when propagating in the access port was the primary cause of the gyrotron perturbation.

III. IMPROVED RECEIVING SYSTEM

The receiver we started with in the CTS experiment in FTU was an evolution of the one formerly used in CTS on the W7-AS stellarator, where millimeter-wave CTS in a fusion-relevant plasma was first demonstrated.[6] The receiving system discussed in this work in turn is the result of a further significant evolution of the system made mandatory by stricter requirements related to the investigation of the anomalous spectra.

A. Multi-input front end

The larger operational flexibility that was required in the investigation of the anomalous spectra was achieved implementing a multi-input front end. As shown in the block scheme of Fig. 4, the input to the receiver could be alternatively taken from (a) the FTU plasma, for CTS and electron cyclotron emission (ECE) measurements; (b) a pick-up line connected to the high-power transmission line propagating the beam from the gyrotron to the plasma, for frequency and input spectrum measurements (see the following); (c) a blackbody source, for receiver calibration purposes; (d) one of two low-power sources, either a 140 GHz IMPATT or a harmonic multiplier driven by a synthesizer, for quick checks of the notch filter (NF) response (see the following).

As seen in Fig. 4, in addition to a number of switches providing path selection according to a given input, two NFs are accommodated in the front-end panel. A NF is always inserted at the input of a CTS receiver to provide high rejection of the stray radiation from the gyrotron. The two NFs, expressly designed for application in CTS in FTU,[7] are quite similar and each consists of a fundamental waveguide

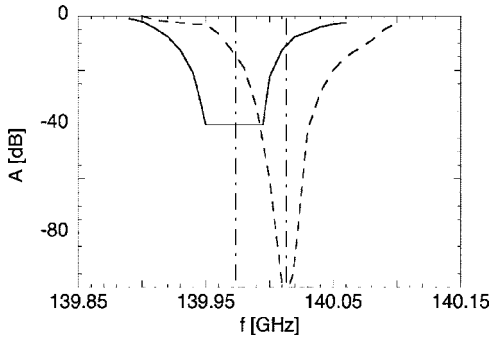

FIG. 5. Typical NF responses. The curve at the right shows the NF response originally obtained in laboratory using a high-sensitivity apparatus, thanks to which the full dynamic range of 100 dB could be covered. The curve at the left refers to the result of a successive retuning of the same NF aimed at matching its central frequency ($f_{\mathrm{NF},0}$) to a measured value of the gyrotron frequency (f_{gyr}). As seen, the dynamic range now is limited to 40 dB by the measuring apparatus.

coupled to 20 cylindrical cavities operating in the H_{013} mode.[8] Their tuning is made possible by trimmers set at each cavity. The attenuation provided is in both cases as high as $\cong$100 dB at the peak of the frequency response and $\geq$40 dB in a ±20 MHz bandwidth (see Fig. 5). Outside a 150 MHz bandwidth the residual attenuation (insertion loss) does not exceed 2 dB. The scope of having two similar NFs available was to allow measurements both at full and reduced (half) gyrotron power. The two NFs are tuned at slightly different frequencies to account for the dependence of gyrotron frequency on the output power level. In Fig. 4 it is also seen that they can be bypassed whenever required, as for instance in the measurements of the gyrotron frequency by the CTS receiver itself (see below).

B. Pick-up line

Measurements of both the gyrotron frequency and the gyrotron spectrum before accessing the plasma were made possible thanks to the implementation of what we briefly label a "pick-up line," made of a rectangular oversized waveguide and also schematically shown in Fig. 1. The signal is picked up by a directional coupler[9] integrated in a miter bend of the high-power transmission line and including a liner array of pinholes, and then, after propagation in the pick-up line, directly illuminates the rectangular horn set at the receiver input. Switching between this signal and any other signal from the multi-input front end is allowed by a simple movable mirror. The required unidirectionality of the measurements with the pick-up line was granted because, while the signals propagating from the gyrotron to the plasma are collected directly, all spurious signals propagating in the opposite direction are necessarily collected through a multiple wall reflection process and therefore attenuated by at least 50 dB due to antenna decoupling.

The measurements of the gyrotron frequency (f_{gyr}) by the receiver itself are described in Sec. V. The measurements of the gyrotron noise spectrum in the presence of the plasma but before accessing it proved decisive in demonstrating the gyrotron origin of the anomalous spectra. They also provided the experimental source function required to perform deconvolutions of the measured spectra in attempts of extracting the ion thermal feature merged in them, as also briefly discussed in Sec. V.

In the experimental campaigns referred to here, the measurements by the pick-up line were alternative to all other measurements. In consideration of their importance, and particularly to make f_{gyr} measurable shot by shot, they will be reorganized using a separate receiver. An upgrade of the pick-up line aimed at increasing its sensitivity to allow measurements of the unperturbed gyrotron noise spectrum in shots performed in the absence of plasma is also underway. The power level to be made available at the receiver input, $\approx$100 mW, corresponding to $\approx 3\times10^{-5}$ % of the beam power, will be obtained by a suitable modification of the linear array of pinholes in the directional coupler described in Ref. 9.

C. High-frequency down-converter

A block scheme of the high-frequency (HF) section of the CTS receiver is shown in Fig. 6. The input level is controlled by a combination of a PIN diode used as voltage-controlled attenuator, with attenuation variable in the range 3–50 dB, and a rotary vane attenuator, with attenuation 0 –50 dB. The PIN attenuator is aimed at allowing remote control of the input attenuation. The rotary vane attenuator, already present in the older scheme, was added to the voltage-controlled PIN attenuator, instead of replacing it, both for extending the dynamic range and for receiver pro-

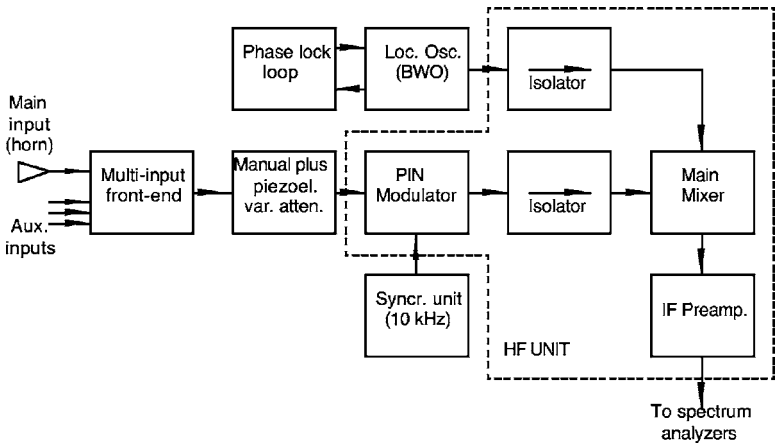

FIG. 6. Block scheme of the HF section of the CTS receiver.

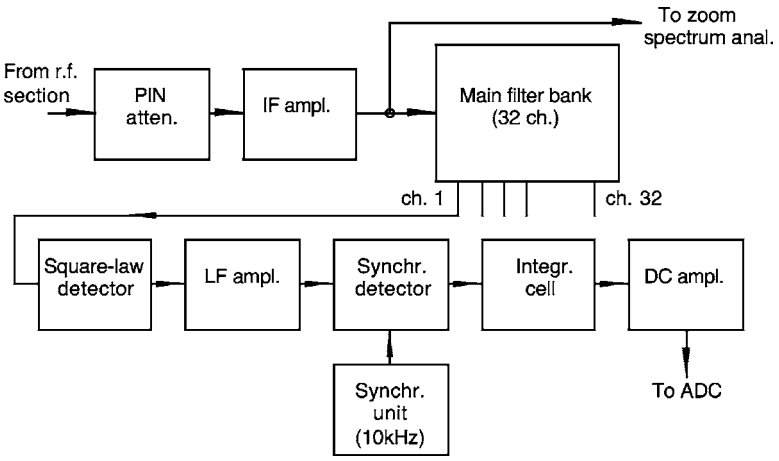

FIG. 7. Block scheme of the IF and LF sections of the CTS receiver. The LF chains that follow the zoom spectrum analyzer (not shown) are similar to those of the main analyzer.

tection reasons, the attenuation provided by PIN attenuator being null for zero control voltage.

Further protection against the stray radiation and any other spurious signals is provided by a second PIN diode inserted just before the main mixer, which now acts as a switch and modulator. This diode is normally kept closed, which corresponds to $\cong$40 dB attenuation, and is open only inside the gate that fixes the measurement time. The residual attenuation it introduces in on state is $\leq$3 dB. The modulation of the input signal is at 10 kHz. Worth being mentioned are also two isolators, with −25 dB isolation, installed between the modulator and the mixer and between the mixer and the local oscillator (LO). A further increase in stray-radiation rejection is produced by an additional high-pass filter (not shown in Fig. 6), with 45 MHz bandwidth, inserted after the first intermediate-frequency (IF) amplifier.

A specification is worth giving on the down-conversion scheme. Homodyne conversion, with the LO frequency set to $f_{LO}=f_{gyr}$, is conveniently used in ion thermal CTS since the ion velocities are isotropic, hence the spectra symmetric with respect to f_{gyr}. Sideband overlap in the detected spectra doubles the sensitivity. However, in pure homodyne detection the LO signal is provided by the carrier, the role of which in the CTS spectra is played by the stray radiation, which is scarcely controllable and therefore totally unsuited to this purpose. A suitably stabilized real oscillator is therefore better used to provide the LO signal in what we label "quasi-homodyne" detection mode. In CTS in FTU we use a backward wave oscillator (BWO) stabilized by a phase-locking loop (PLL) based on a harmonic mixer operating at the 21st harmonic and driven by a synthesizer with 10^{-8} accuracy and output frequency adjustable down to 1 kHz steps.

D. Intermediate-frequency section

In the intermediate-frequency (IF) section of the CTS receiver (see Fig. 7) spectral analysis is performed by a spectrum analyzer including 32 adjacent channels ($j=1-32$) with constant relative selectivity, $\Delta f_j/f_{0,j}=\beta$, with $\beta=0.1$. The progressively increasing channel widths this implies are aimed at providing a compensation for the reduction of the signal-to-noise ratio (SNR) with increasing frequency, while maximizing frequency resolution at low frequency consistently with the criticality of this spectral region. The central frequency chosen for the first channel, $f_{0,1}=50$ MHz, accounts for the frequency interval to be excluded from the measurements due to the finite (non-negligible) insertion loss of the NF. The measurement bandwidth made available in the conditions summarized above, 50–1200 MHz, largely exceeds the ion thermal bandwidth expected to be measured, as required. As in the HF section, the input of the IF section is controlled by a PIN modulator.

Opposite to the early experimentation, where they were suspected to be ascribable to plasma-wave interactions, in investigating the anomalous spectra in terms of gyrotron perturbation our interest was mostly focused on their global behavior. Nevertheless, finely resolving single lines (actually, spectral peaks) was still useful, e.g., to assess whether the line frequencies were recurrent as we expected consistently with the gyrotron perturbation hypothesis. For this purpose in the initial version of the receiver we used a "zoom" spectrum analyzer with 32 channels of constant absolute selectivity and 3 MHz width, operated in parallel to the main analyzer. The analysis band available in a shot was 100 MHz. This band could be allocated in eight different positions, each with 50 MHz separation, by manual switching of the LO frequency of a down-converter included in the analyzer. The analysis band above, however, often proved inadequate to meet our needs. Moreover, less than one half of the measurement bandwidth could be covered on a shot-to-shot basis.

To overcome these limitations a new zoom spectrum analyzer of more advanced conception, in particular with improved suppression of ghost signals, was designed and implemented. A block scheme of it is shown in Fig. 8. There are still 32 channels, but now their width is enlarged to 5 MHz. Further, the analysis band is extended to 160 MHz and can be allocated in 11 positions, each separated by 160 MHz. This made the total bandwidth coverable on a shot-to-shot basis equal to the measurement bandwidth (1.2 GHz) as required.

E. Low-frequency section and DAS

The low-frequency (LF) section (see Fig. 7) consists of 32 channel chains, each of which includes a square-law detector, a low-frequency amplifier, a synchronous detector

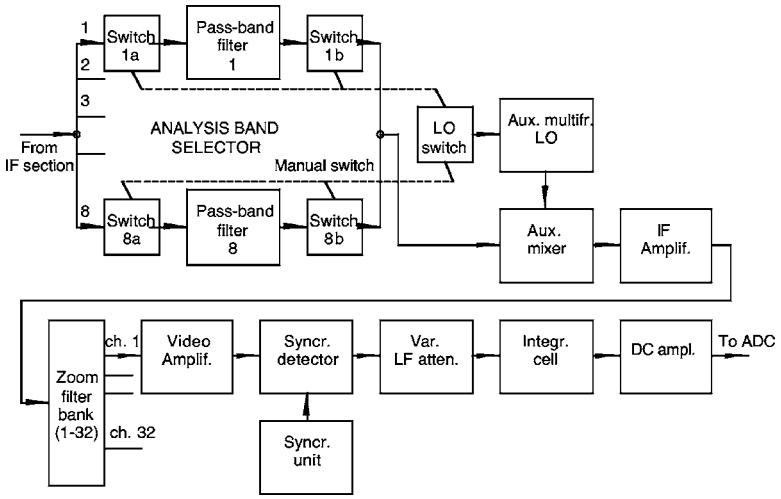

FIG. 8. Block scheme of the improved zoom spectrum analyzer.

with modulation at 10 kHz, a low-pass (RC) filter with time constant of 1 ms, and a dc amplifier. The dc signals of the (32+32) channels of the main and the zoom analyzers are finally digitized and send to the central data acquisition system (DAS) of FTU.

F. Remote control of receiver parameters

Being accommodated in a controlled area near the tokamak hall, the CTS receiver was inaccessible during the experimentation. To overcome the limitations this introduced, remote control of the receiver parameters of most frequent use was implemented, linking the receiver to a programmable logic controller (PLC) connected to the plant-control system.

Remote control of the input attenuation was made possible by the already-mentioned voltage-controlled PIN attenuator. The synthesizer frequency could be remotely assigned in digital form. The six digits available provided an accuracy of ±200 kHz in absolute terms, corresponding to $\cong 10^{-7}$ in relative terms. Thanks to remote control, operation of the PLL in nonlocked conditions, e.g., with either temporary or persistent loss of the frequency lock, was also fully prevented. Finally, operation of the front end in potentially dangerous configurations was prevented thanks to a software-controlled possibility of remotely checking the working configuration.

G. Receiver calibration and performances

The digitized dc voltage measured at the output of each of the LF channel chains is related to the "antenna temperature" of the channel, $T_{\text{ant},j}=P_{\text{ant},j}/\Delta f_j$, by the relation

$$\overline{V}_j = c_j(T_{\text{ant},j} - T_0) + \overline{\Delta V}_j, \tag{3}$$

where $\overline{V}_j$ is the channel voltage integrated over an integration time τ_{int} (see the following), the c_j transmission (or calibration) coefficients, $\overline{\Delta V}_j$ a residual channel voltage of technical origin, and T_0 a "room" temperature corresponding to the closed state of the PIN modulator at the receiver input.

The coefficients c_j and $\overline{\Delta V}_j$ are determined by receiver calibration with a source of known temperature. In our case the calibration was performed using either a gas discharge with blackbody emission in the frequency range of interest ($T_{\text{bb}}=0.4$ eV) or the ECE from a "resonant" ($B_T=5$ T) plasma ($T_{\text{bb}}=T_e\cong 1$ keV) at high enough density to make it optically thick for both plasma modes in the propagation conditions of interest. The temperature available being quite low, the calibration by the blackbody source was used mainly to check if the conditions of optical thickness were satisfied by a given plasma target. The much more convenient calibration by ECE was routinely used in the experimentation.

Accounting for the "noise" contributions (namely, all signals of non-CTS origin) to the input, we further have

$$T_{\text{ant},j} = T_{\text{CTS}\,j} + T_{\text{ECE}} + T_{\text{gyr},j} + A_{\text{in}}T_{\text{rec}}, \tag{4}$$

with $T_{\text{CTS},j}$ the temperature of the scattered signal, T_{ECE} the radiative temperature of the ECE background, $T_{\text{gyr},j}$ an equivalent gyrotron noise temperature further discussed later on, and $A_{\text{in}}T_{\text{rec}}$ the receiver noise temperature transferred to the antenna input, A_{in} being the total attenuation between the antenna and the mixer inclusive of the HF attenuation. As already mentioned, in the FTU case $\overline{T}_{\text{CTS}}\cong 100-500$ eV, which is to be compared with an equivalent receiver noise at the mixer input of $T_{\text{rec}}\cong 0.4$ eV and, with reference to plasmas at the magnetic field of most frequent use ($B_T=7.2$ T), an ECE background of $T_{\text{ECE}}\cong 30-50$ eV. The advantage of low ECE noise is typical of CTS with $f_{\text{gyr}}<f_{\text{ec}}$. The gyrotron contribution $T_{\text{gyr},j}$ was everywhere negligible.

As relation (4) shows, the temperature of the total noise, $T_{n,j}=T_{\text{ECE}}+T_{\text{gyr},j}+A_{\text{in}}T_{\text{rec}}$, can be obtained from measurements with $T_{\text{CTS},j}=0$, i.e., either from shots performed in absence of the gyrotron beam (provided $T_{\text{gyr},j}$ is negligible as it was our case), or directly reading the signal in the highest channels such that $T_{\text{CTS},j}=0$ for $j>m$ in the CTS measurements themselves. The temperature of the scattered signal in the jth channel, $T_{\text{CTS},j}$, is then readily recovered using (4).

Estimates of the SNR achieved in a measurement were also obtained using the standard relation

$$\text{SNR}_j = T_{\text{CTS},j}/\langle \delta T_{\text{syst},j}\rangle, \tag{5}$$

where the noise level here is more properly defined in terms of a fluctuation level given by

$$\langle \delta T_{\mathrm{syst},\,j} \rangle = T_{\mathrm{ant},\,j} / \sqrt{\Delta f_j \tau_{\mathrm{int}}}, \tag{6}$$

with $T_{\mathrm{ant},\,j}$ given by (4), Δf_j the jth channel bandwidth, and $\tau_{\mathrm{int}} = \tau_{\mathrm{RC}} + \tau_{\mathrm{soft}}$ an integration time given by the sum of the time constant of the RC cell (τ_{RC}) and a contribution set via software (τ_{soft}), with $\tau_{\mathrm{int}} \geq 1$ ms. It is easily checked from the signal and noise temperatures given above that in the conditions of CTS of FTU the SNR is typically very high (≥ 100).

IV. CRITICAL ISSUES EMERGING IN THE INVESTIGATION

In this section we discuss the critical issues that were at the origin of the improvements described above and were overcome by the operating procedures described in Sec. V.

A. Suitability of the gyrotron performances

In CTS the stability in frequency of the probing source is required to be at least one order of magnitude higher than the fractional bandwidth involved, in our case $\Delta f_{\mathrm{CTS}}/f_{\mathrm{gyr}} \approx (2-4) \times 10^{-3}$. The frequency measurements described in Sec. V confirmed that in CTS in FTU this criterion was largely satisfied since $\Delta f/f_{\mathrm{gyr}} \approx 5 \times 10^{-5}$. Also mandatory in CTS experiments is the requirement of good spectral purity, i.e., of total absence of satellite lines in the gyrotron output. In our gyrotron this was so in "normal" operating conditions, namely in shots performed in the absence of plasma. In contrast, in a broad sense the lines in the anomalous spectra may be seen as satellites initial transient of the gyrotron frequency from higher to lower values is unavoidable because of thermal dilation in the resonant cavity. The duration of this transient however is strongly sample dependent. Gyrotron samples with transient times of hundreds of milliseconds are definitely unsuited for use in CTS. The transient time is in any case better excluded from the CTS measurements due to the unacceptable mismatch it produces with respect to the NF frequency. In CTS in FTU this is obtained triggering the gate that is applied to the PIN modulator set at the receiver input with a software-controllable delay (blind time) slightly exceeding the typical transient time, 20–30 ms.

The noise spectrum of a gyrotron originates from several "natural" noise sources as the shot noise, related to the discreteness of the emitting electrons, the thermal noise, related to cyclotron emission, etc. In the strict vicinity of the main line, the spectral region of interest here, however, the main noise contribution comes by large from more "technical" factors, e.g., the conversion of phase noise into amplitude noise. A common feature of all forms of gyrotron noise is in any case their being by definition non-Gaussian, i.e., their exhibiting rms fluctuations definitely higher than in the Gaussian case. Accordingly, the ratio of the equivalent gyrotron noise temperature defined above ($T_{\mathrm{gyr},\,j}$) to the underlying fluctuation is also different and less favorable than for the other noises. Whenever non-negligible, therefore, the gyrotron noise will make the SNR evaluated from relations (5) and (6) overestimated and actually unknown, the actual fluctuation level being unknown. Besides this, due to its strongly frequency dependence, subtraction of this noise from the measured spectrum will become necessary to properly recover the shape of the latter.

This explains why conditions of negligible gyrotron noise are pursued as far as possible in CTS experiments empirically assuming that whenever $T_{\mathrm{gyr},\,j}$, is negligible in all channels the associated fluctuation level will also be negligible in proportion. In ion thermal CTS achieving these negligibility conditions is generally not difficult. More difficult can be achieving them in the more advanced experiments of CTS on fast ion tails (FITs),[10] the scattered signal there being at least two orders of magnitude lower and the spectral shape associated with FITs often approaching that of the gyrotron noise spectrum itself. Measurements of the gyrotron noise spectrum in absence of plasma confirmed that in our case the gyrotron noise temperature was negligible ($T_{\mathrm{gyr},\,j} \leq 1$ eV) in all channels for $f_{0,j} > 100$ MHz.

These good performances both in transient time and in terms of noise were greatly facilitated by the possibility of selecting our gyrotron amoung four available for electron cyclotron heating (ECRH) and current drive (ECCD) applications. Concerns were nevertheless present as regards the *stability* of the noise level in consideration of the predicted high sensitivity of millimeter-wave gyrotrons to perturbing signals and nonoptimized operating conditions. A warning in this sense was provided by the strict similarity in shape of the gyrotron noise spectrum in unperturbed conditions and the smooth low-frequency feature exhibited by all the anomalous spectra. Further, in tests aimed at investigating a possible role of the stray radiation in producing these spectra, where the gyrotron was forced to operate at about half the maximum power, slightly changing its working parameters, which accordingly were no more optimized, an increase of the noise spectrum by about one order of magnitude was systematically observed.

This evidence led us to focus our attention on checking if and how the ion thermal feature merged in the anomalous spectra could be recovered, first from the simplest of them, as the one shown in Fig. 2, and then from the spectra of any type, including those with more or less complex line structures. Indeed, this would have provided a reasonable outcome in all cases where the gyrotron perturbation could be contained but not fully suppressed. To this purpose, the Dirac delta implicitly assumed in the standard treatment of CTS had to be replaced by an experimental source function and a deconvolution of the measured spectra had to be performed taking this function as kernel.

Deconvolutions of the measured spectra were effectively tried using a dedicated numerical routine and the source function made available by the measurements with the signal taken from the pick-up line described in Sec. III. However, due to the many-orders-of-magnitude difference in the spectral strengths involved even with the weakest of the spectra, and to the lack of calibration of the source function, the results were only partially successful. The deconvoluted spectra were definitely "nonempty," as expected, and their bandwidth finely approached the predicted one, but the spectral shapes were only very roughly those expected for the ion thermal feature even discounting that a large uncertainty was

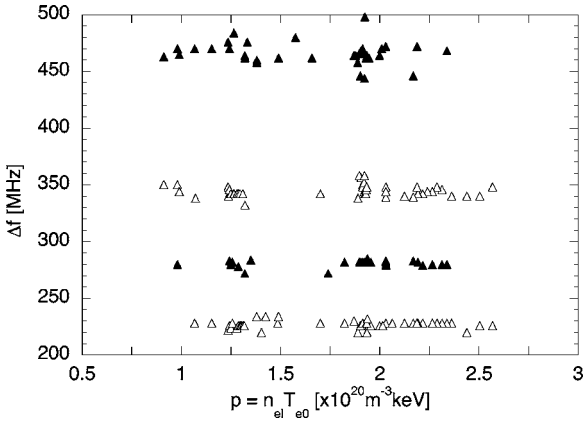

FIG. 9. Estimated line frequencies, with $f_{\mathrm{line}}=f_{\mathrm{gyr}}\pm\Delta f$, in the lower half of the measurement bandwidth, ordered vs plasma pressure. Sideband overlap is not taken into account. The error bars are approximately equal to half the width of the channel that is nearest to the estimated line frequency, $\delta\Delta f \cong \pm 0.05\Delta f_{\mathrm{ch}}$. The frequency values are obtained by interpolation of the experimental points by a cubic spline procedure. The alternating black and white triangles refer to a tentative assignment of the estimated frequencies to a given line to provide an idea of the rate of occurrence of the lines.

present since the low-frequency contributions from the plasma impurities were unknown. Preliminary indications on how to perform ion temperature measurements even in presence of a *slight* perturbation of the gyrotron output are nevertheless provided by this special form of signal processing.

B. Insufficiencies in spectral resolution

Of considerable importance in the investigation of the anomalous spectra was checking if and to what extent the frequencies of the spectral lines detected were recurrent as expected in the frame of the gyrotron perturbation hypothesis. Particularly at high frequencies, however, the channel partition specified in Sec. III was quite unfit to finely resolve the spectral peaks, e.g., to check if they were actually line patterns. More suited were the uniformly distributed narrow channels of the zoom spectrum analyzer but, as already mentioned, in this case only a small fraction of the spectral width could be covered in a single shot.

In spite of these limitations, the recurrent character of the line frequencies could be confirmed, even if only statistically. In Figs. 9 and 10 the estimated frequencies, $\Delta f = |f_{\mathrm{gyr}} \pm f_{\mathrm{line}}|$, of the spectral peaks detected in a high number of anomalous spectra are plotted taking the plasma pressure as independent parameter for convenience. The spectral power densities of these lines varied by more than one order of magnitude and only a few of them were simultaneously present in a given spectrum. Due to sideband overlap, moreover, the line frequencies can be either $f_{\mathrm{line}}=f_{\mathrm{gyr}}-\Delta f$ or $f_{\mathrm{line}}=f_{\mathrm{gyr}}+\Delta f$. Nevertheless, the recurrent character of the lines is quite manifest, especially in Fig. 9. The larger scattering of the data in Fig. 10 reflects a larger uncertainty related to the channel widths becoming progressively wider.

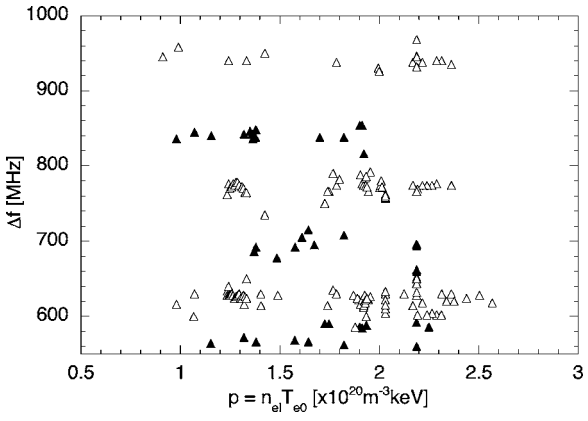

FIG. 10. Same as in Fig. 9 in the upper half of the measurement bandwidth.

An additional limitation, particularly heavy in our initial attempts of explaining the anomalous spectra in terms of plasma-wave interactions, was that sideband overlap made us unable to assess the symmetry of the spectral lines, i.e., if they were double- or single-sided and, in the latter case, if they pertained to the lower or the upper sideband of the complete (double-sided) spectrum. This limitation was overcome, and a confirmation of the expected double-sided character of the lines was obtained, operating the receiver in the slightly heterodyne mode described in Sec. V.

C. Stray-radiation and receiver saturation problems

A rejection capability of at least 80–90 dB at f_{gyr} (stray radiation) is required for safe CTS operation. Antenna decoupling hardly exceeding 50–60 dB, the additional attenuation is provided by the NF already described. Some mismatch of the gyrotron and the central NF frequencies ($f_{\mathrm{gyr}}=f_{\mathrm{NF},0}\pm\delta f_{\mathrm{mism}}$) being unavoidable, however, the attenuation effectively made available by the NF is currently much lower than the maximum seen in Fig. 5. An average NF attenuation not exceeding 30–40 dB was assumed in designing the CTS experiment in FTU.

While adequate for detecting ion thermal spectra, these conditions were much less so as regards the investigation of anomalous spectra. The risk of partial or even total misinterpretation of the data due to some of the receiver stages operating outside its linear range due to unrecognized high stray-radiation levels was much higher. Further, undetected saturation effects could have been produced, the strengths of the spectral features varying by orders of magnitude in shots performed in different plasma or beam polarization conditions. As an example of the complexity of IF saturation effects we mention periodic (10 kHz) degradation of the amplified signal in one or several channels. The periodicity is related to the absence of saturation when the PIN modulator set at the receiver input is closed. The modulation being in antiphase with the input signal, a seemingly totally unnatural consequence of this form of saturation is the appearance of negative signals in other (nonsaturated) channels.

The absence of negative signals was one of the criteria we adopted for properly adjusting the attenuations in the IF and LF stages. Concerns nevertheless remained as regards the possibility that all or some of the spectral lines, if not the anomalous spectra as such, were artifacts related to only partially recognized, or not well understood, saturation effects caused by either the stray radiation or the spectral lines. For instance, a strong increase of the stray radiation leading to

unrecognized receiver saturation might have been produced in case of turbulent scattering on the injected beam occuring at the plasma periphery.

To prevent its possibly causing saturation effects, the stray-radiation level was made thoroughly checkable by installing a calibrated detector, with 10 dB decoupling, in the propagation path in between the last mirror of the quasi-optical transmission line and the input horn. The detector signal was digitized in parallel to the data to make it remotely available shot by shot. Further, and still more important, stray-radiation rejection was pushed to a maximum by the frequency-matching procedure described in Sec. V. These new operating conditions definitely confirmed that the anomalous spectra were not associated with increased stray-radiation levels. Saturation effects due to strong spectral lines becoming exceedingly strong were also quite easily prevented thanks to the controllability of the input level over a 60 dB range allowed by the two variable attenuators set at the receiver input.

V. NEW OPERATING PROCEDURES

In this section we describe the new operating procedures introduced to make the upgraded receiver match the stricter demands that emerged in the investigation of the anomalous spectra.

A. Receiver operation in slightly heterodyne mode

Receiver operation in what we briefly label "slightly heterodyne" mode, i.e., with f_{LO} shifted by a preset amount with respect to its quasi-homodyne value, was profitably used for a number of purposes. Common to all was that the spectral feature under investigation was placed in the channel most suitable to optimize the measurement. For instance, moving a spectral line to one of the lowest channels, typically the second or the third, improved its resolution by more than one order of magnitude. Operation in the slightly heterodyne mode was successfully exploited: (a) to assess the symmetry of the spectral lines; (b) to quickly check $f_{\mathrm{NF},0}$; (c) to measure f_{gyr} using the CTS receiver itself.

The symmetry of the spectral lines was assessed simply by observing the shift of the line and of its image in the complementary sideband, if any, at suitably shifted f_{LO} values. To optimize the result the measurement was usually iterated a few times, shifting f_{LO} by a small amount shot by shot. The overall shift of f_{LO} was required to be in any case larger than the linewidth, $\Delta f_{\mathrm{LO}} > \Delta f_{\mathrm{line}}$. The expected double-sided character of the spectral lines was clearly confirmed by these tests.

Either complete retuning or quick checks of $f_{\mathrm{NF},0}$ were obtained by two methods, the first of which quite accurate but performed off-line, and the second faster and performed on-line, still exploiting slightly heterodyne operation. In the first method the testing signal was provided by a harmonic mixer acting as a multiplier and driven by an independent synthesizer, the frequency of which was swept sinusoidally. The signal was detected using one of the CTS channels. This method provided the full NF response within a 40 dB dynamics (see the response at left in Fig. 5), from which $f_{\mathrm{NF},0}$ was readily evaluated. When useful, the symmetry of the two wings of the NF response could be improved slightly retuning some of the resonant cavities in a cut and try procedure.

In the second method, resonant ($B_T = 5$ T) ohmic plasmas was exploited to provide a wideband generator. The spectral response here was obtained comparing (subtracting from one another) the spectra produced in two shots, one of which performed with the NF inserted and the other with NF bypassed. In these measurements the shift of f_{LO} was chosen such as to put the last measured value of f_{gyr} at the center of the measurement bandwidth, i.e., $\Delta f_{\mathrm{LO}} \cong \Delta f_{\mathrm{det}}/2 = 600$ MHz. No problems arose as regards the stability of the BWO in these conditions. Due to sideband overlap, the spectral dynamics now was limited to 3 dB, but nevertheless the $f_{\mathrm{NF},0}$ value could be easily read after suitable scale expansion. The main advantages of this method resides in its being applicable on-line. Whenever a significant lack of symmetry in the NF response was evidenced, we switched to the more accurate off-line method.

To measure f_{gyr}, gyrotron shots were performed in the vacuum vessel with the signal taken from the pick-up line and the NF bypassed. The ambiguity related to sideband overlap was avoided operating in the upper sideband, i.e., with $f_{\mathrm{LO}} < f_{\mathrm{gyr}}$. Here too, some iterations of the measurement, with the f_{LO} value adjusted shot by shot, were normally required in order to make the gyrotron line fall in one of the lowest channels, to maximize the spectral resolution, as well as to optimize the result, e.g., to avoid the gyrotron line falling in between two channels. The accuracy achieved, estimated as half the channel width, was $\pm(2.5-3.5)$ MHz for measurements performed, respectively, in the second and the third channel. A high accuracy (± 2.5 MHz) was obtained also in the similar measurements with the zoom spectrum analyzer. However, these only occasionally replaced those with the main analyzer due to their being more wearisome.

B. Frequency-matching procedure

Besides their intrinsic usefulness, the measurements of $f_{\mathrm{NF},0}$ and f_{gyr} described above were exploited also to finely match these frequencies in order to jointly maximize the NF attenuation and spectral symmetry in sideband overlap. Maximizing stray-radiation rejection provided an answer to most of the issues discussed in Sec. IV. A high degree of symmetry in sideband overlap minimized the spectral distortion in the very low-frequency region, where the residual attenuation of the NF is small but not yet negligible. This made the comparison of the smooth, low-frequency feature present in the anomalous spectra with the gyrotron noise spectrum much more accurate. The strict similarity of their shapes was confirmed.

First $f_{\mathrm{NF},0}$ was checked by one of the two methods mentioned above and then f_{gyr} was matched to the measured value of the former frequency. The small variation in frequency this required was produced by slightly varying the current of the gyrotron magnet. The variation required was always lower than 1%. The tuning range to be covered never exceeded $\Delta f/f_{\mathrm{gyr}} = \pm 4 \times 10^{-4}$. The variation in the output power ($P_{\mathrm{gyr}} \propto \Delta f_{\mathrm{gyr}}^{-1}$) was largely acceptable in all cases. The estimated accuracy in frequency, hence in sideband overlap

as well, is ±5 MHz. Neglecting possible signal leakage, the stray-radiation rejection level achieved, evaluated as the sum of the NF attenuation and antenna decoupling, was as high as 120–140 dB at $A_{in}=0$.

In a typical experimental session the frequency-matching procedure was actuated just after the two calibration shots in ohmic plasmas used to quickly check $f_{NF,0}$. To update the transmission coefficients (c_j) in optimized conditions then receiver calibration was repeated using a third plasma shot.

VI. DISCUSSION AND CONCLUSIONS

As already mentioned, at the origin of the anomalous spectra observed in CTS in FTU was a power fraction polarized in the *X* mode in the gyrotron beam when propagating in the access port. In principle, therefore, the perturbation exciting these spectra would be avoidable, without changing the layout, simply by recourse to fine polarization control. Indeed, adjusting the incident polarization so as to provide propagation in the pure ordinary (O) mode when crossing the RH cut-off would make it latent and therefore suppress the back-reflection.

To achieve this goal, however, the injected beam should be given an elliptical polarization with parameters consistent with the mode partition corresponding to the *local* propagation conditions and this is rather difficult to do for a number of reasons. The propagation direction in the port may change considerably in passing from one of the antenna mirrors to the other. While particularly strong in the case of the multimirror antenna used for CTS in FTU, these changes are present in most antenna systems. Besides this, the spatial distribution of the magnetic field lines in the port is generallly only roughly known. This further contributes to make the pitch angle, and therefore the polarization setting required to provide *O* mode propagation at the RH cutoff layer, quite uncertain. Moreover, even once these provisions are taken, the gyrotron may still be perturbed due to occasional errors or inaccuracies in setting the polarization. The improvements and the operating procedures discussed above therefore would remain useful even if the solution envisaged above is adopted.

Relying solely on a proper polarization setting would be still more inadequate as regards the final aim of CTS in FTU of demonstrating high-density CTS with *X* mode propagation, as of interest for ITER The pitch angle in the beam injection port and in the plasma being in all cases different, pure *O* mode propagation in the former is incompatible with pure *X* mode propagation in the latter. This is the strongest reason why, in CTS with $f_{gyr}<f_{ec}$, the transmitting antenna must be made *a priori* robust against the risk of gyrotron perturbation. To this purpose, the use of evacuated transmitting antenna has been proposed in Ref. 3. In particular, an evacuated remote steering antenna[11] of symmetric type[12] is being considered for implementation in FTU.

Even if a safe solution for the transmitting antenna is adopted, as long as a CTS experiment is proof-of-principle, namely operated in conditions never explored before, equipping the receiving system as indicated in this work will be still convenient, even if no more mandatory, in order to make it able to cope with possible unwanted (coherent) plasma-wave processes, of which, as already mentioned, the anomalous spectra are to a large extent representative. At high enough power densities a single plasma-wave system with a nonlinear dielectric response must be considered. In these conditions the free energy associated with the pump wave can drive a wide spectrum of processes. Only the probability of their taking place in a given experiment, a given fusion-relevant plasma, and within the measurement bandwidth involved is questionable. It is true that the experimental evidence seems to indicate that so far these unwanted processes have never been a problem. However, the number of experiments of "thermal" (nonturbulent) CTS carried out at high enough power levels (hundreds of kW), including both those already completed (JET,[13] W7-AS[14]) and those still ongoing (Textor,[15] Asdex Upgrade,[16] FTU), is still small and therefore the statistics poor and not really conclusive. Moreover, in the longer term account must be taken of the power levels up to ten times higher (MW) envisaged for the CTS diagnostic of the confined alphas in ITER.[2]

In this far-sighted perspective, and in spite of their having been actuated in the frame of quasi-homodyne detection, the use of which is limited to ion thermal CTS, the upgrade of the receiver and the operating procedures discussed in this work provide both a warning on the necessity of coping with the additional goals stressed above and preliminary indications on how to do that with limited extensions of the standard system.

[1] F. Orsitto, A. Brusadin, Yu. Brodsky, S. Filchenkov, G. Grosso, E. Giovannozzi, L. Lubyako, A. Perminov, E. V. Suvorov, U. Tartari, and F. Volpe, Rev. Sci. Instrum. **70**, 1158 (1999).
[2] H. Bindslev, F. Meo, and S. Korsholm, "ITER Fast Ion Collective Thomson Scattering–Feasibility Study," Annex 1, Riso Lab. Report under EFDA Contract 01.654, November 2003. ITER is a tokamak project based on a worldwide collaboration and aimed at demonstrating controlled ignition. The construction of the device is now being started in France.
[3] U. Tartari, G. Grosso, G. Granucci, L. V. Lubyako, A. G. Shalashov, E. V. Suvorov, F. P. Orsitto, A. Simonetto, S. Nowak, F. Volpe, A. Bruschi, F. Gandini, V. Muzzini, S. Garavaglia, and G. Grossetti, Nucl. Fusion **46**, 928 (2006).
[4] J. Sheffield, *Plasma Scattering of Electromagnetic Radiation* (Academic, New York, 1975).
[5] U. Tartari, G. Grosso, and S. Nowak, Rev. Sci. Instrum. **70**, 1162 (1999).
[6] L. V. Lubyako, E. V. Suvorov, A. B. Burov, A. M. Shtanyuk, Yu. A. Dryagin, L. M. Kukin, and N. K. Skalyga, Tech. Phys. **43**, 926 (1998).
[7] We acknowledge this important contribution from our dear friend Dr. Yu. A. Dryagin, who recently died.
[8] Yu. A. Dryagin, N. Skalyga, and T. Geist, Int. J. Infrared Millim. Waves **17**, 1199 (1996).
[9] A. Simonetto, G. Solari, F. Gandini, G. Granucci, V. Muzzini, and C. Sozzi, Fusion Sci. Technol. **40**, 247 (2001).
[10] See, for example, F. Meo, H. Bindslev, S. B. Korsholm, E. L. Tsakadze, C. I. Walker, P. Woskov, and G. Vayakis, Rev. Sci. Instrum. **75**, 3585 (2004).
[11] See, for example, W. Kasparek, G. Gantenbein, B. Plaum, R. Wacker, A. V. Chirkov, G. G. Denisov, S. V. Kuzikov, K. Ohkubo, F. Hollmann, and D. Wagner, Nucl. Fusion **43**, 1505 (2003).
[12] Of special interest for FTU is the symmetric remote steering antenna successfully tested in the TRIAM-1M device. See H. Idei, K. Hanada, H. Zushi, K. Ohkubo, M. Hasegawa, S. Kubo, S. Nishi, A. Fukuyama, K. N. Sato, K. Nakamura, M. Sakamoto, A. Iyomasa, S. Kawasaki, H. Nakashima, A. Nigashijima, T. Notake, T. Shimozuma, S. Ito, H. Hoshika, N. Maezono, K. Nakashima, and M. Ogawa, Nucl. Fusion **46**, 489 (2006).
[13] H. Bindslev, J. A. Hoekzema, J. Egedal, J. A. Fessey, T. P. Hughes, and J. S. Machuzak, Phys. Rev. Lett. **83**, 3206 (1999).
[14] E. V. Suvorov, E. Holzhauer, W. Kasparek, L. V. Lubyako, A. B. Burov,

Y. A. Dryagin, S. E. Filchenkov, A. A. Fraiman, L. M. Kukin, A. V. Kostrov, D. A. Ryndyk, A. M. Shtanyuk, N. K. Skalyga, O. B. Smolyakova, V. Eckmann, T. Geist, M. Kick, H. Laqua, and M. Rust, Plasma Phys. Controlled Fusion **39**, B337 (1997).
[15] H. Bindslev, S. K. Nielsen, L. Porte, J. A. Hoekzema, S. B. Korsholm, F. Meo, P. K. Michelsen, S. Michelsen, J. W. Oosterbeek, E. L. Tsakadze, E. Westerhof, and P. Woskov, Phys. Rev. Lett. **97**, 205005 (2006).
[16] S. Michelsen, S. B. Korsholm, H. Bindslev, F. Meo, P. K. Michelsen, E. L. Tsakadze, J. Egedal, P. Woskov, J. A. Hoekzema, F. Leuterer, and E. Westerhof, Rev. Sci. Instrum. **75**, 3634 (2004).